Surface Corrosion Inhibition of Mild Steel in an Acidic Environment by an Anthelmintic Drug: Experimental, RSM, DFT and MD Simulation Studies

F. O. Edoziuno[1,2]*, B. U. Odoni[1], A. A. Adediran[3,4], S. Byadi[5], A. Barhoumi[6], C. C. Nwaeju[2,7], L. U. Modebe[8] and J. O. Okeniyi[9]

[1]*Department of Metallurgical Engineering, Delta State Polytechnic, Ogwashi-Uku, Nigeria*
[2]*Department of Metallurgical and Materials Engineering, Nnamdi Azikiwe University, Awka, Nigeria*
[3]*Department of Mechanical Engineering, Landmark University, P.O. Box 1001, Omu-Aran, Kwara State, Nigeria*
[4]*Mechanical Engineering Science, University of Johannesburg, South Africa*
[5]*Department of Chemistry, Hassan II University, Casablanca, Morocco*
[6]*Department of Chemistry, Chouaib Doukkali University, El Jadida, Morocco*
[7]*Department of Mechanical Engineering, Nigerian Maritime University, Okerenkoko, Delta State, Nigeria*
[8]*Department of Chemical Engineering, University of Delta, Agbor, Nigeria*
[9]*Department of Mechanical Engineering, Covenant University, Ota, Ogun State, Nigeria*
* Corresponding author: francisedoziuno@gmail.com

Abstract

Gravimetric, electrochemical, surface investigation, RSM and theoretical computational studies, using DFT and MD, were employed to investigate E_{corr} inhibition of MS surfaces in 0.5 M H_2SO_4, by a worm expelling drug (Wormin® MBZ). The results from computational and RSM optimization and experimental methodologies were all in good accord. After 24 h, IE(%) of 1.5 g/L MBZ on MS corrosion, calculated from WL data, was 96.610%. Maximum IE(%) of 1.0 g MBZ was 96.903% (303 K) and 99.998% (333 K). PDP confirmed MBZ mixed nature of adsorption. The impact of the inhibitor C and IT of MS on IE(%) of MBZ was revealed by statistical evaluation and optimization, using Design Expert software package (Stat-Ease). The optimized IE(%) of 96.6103% was obtained with the inhibitor C of 1.061 g/L, at MS 48.58 h IT. On the MS surface, MBZ behaved according to Langmuir's adsorption isotherm. MD showed that MBZ had an $E_{interaction}$ of -536.33 and -694.53 kcal/mol, at 303 and 333 K, respectively. Negative $E_{interaction}$ forecasts confirmed MBZ-MS surface interaction capability, which reinforced the experimental investigations IE(%) findings.

Keywords: adsorption; $C_7H_6N_2$ derivative; DFT; MBZ; MD optimization; RSM; PDP.

Introduction•

Understanding the physical, mechanical and chemical properties of metallic materials is essential for their efficient usage in structural and building

---

• The abbreviations and kinetic parameters lists are in pages 23-24.

applications. The chemical properties of metals cannot be dissociated from the prevailing service environment and conditions [1-3]. Although MS is commonly used for a wide range of industrial applications, because it is readily available at a low cost, and possesses good physical and mechanical properties, it has poor resistance to dissolution in a reactive service environment [4-6]. This has led to increasing investigations on how to mitigate MS corrosion [7, 8]. Corrosion is a type of surface deterioration that occurs when metals are exposed to aggressive environments, due to reactions between them. During many of these industrial processes, MS is exposed to severe corrosive attacks by acid solutions [7, 9-11], such as H_2SO_4, which is widely used in industries for pickling, descaling, acid cleaning, acidizing of oil wells, etc. In order to combat this problem, the use of chemical inhibitors is regarded as one of the most successful techniques, due to their ease of application and cost-effectiveness. However, since most of the compounds examined for CI are either toxic or very expensive, there is a need for further research, in order to identify non-toxic, environmentally benign and inexpensive inhibitors, with good IE(%) at low C [5]. A large array of research publications has outlined and described numerous chemical compounds that possess corrosion protection properties. However, only a few of them have been employed as CI in the industries. To some extent, this is because the properties desired for a CI are not limited to the surface protection of metals in service. of Cost, availability, toxicity and eco-friendliness considerations are paramount, due to the rising global ecological campaigns, tougher environmental regulations and sanctions [5, 9, 11, 13-15].

In water presence, which serves as an ion transport channel, metallic electrochemical corrosion occurs when electrons from atoms on the metal surface are transported onto a suitable electron acceptor. The most common electron acceptors (depolarizers) are O, acids and the cations of less active metals. CI are chemical compounds that interact with metallic surfaces, or with their environment, thereby giving them an amount of protection or corrosion resistance [16-18]. The effectiveness of organic/inorganic CI is largely determined by factors such as the metal and aggressive solution properties, their mode of interaction, the inhibitor molecular and electronic structure, C, solubility, pH and T [5, 19]. The most extensively utilized methods to estimate the molecular reactivity of every inhibitors compounds are DFT and MD simulations [20, 21]. Any fundamental strategy for preventing corrosion must take into account the metal structural properties, the environment, and the reactions that occur between them [21, 22]. Research found that many organic compounds with N, O, P and S heteroatoms and/or with π-electron systems are employed as metals CI in different service environments [7, 10, 23]. These inhibitors adsorb themselves onto the metallic surfaces, thereby changing the electrical double layer structure [5, 11, 24-26], and creating a protective surface film on the metal, which serves as a barrier against the aggressive media [9, 15, 27]. Usually, CI are applied by dispersion, or distributed from a solution. Some of them are integrated into the formulation of protective coatings. They work by accelerating anodic or cathodic polarization behaviour, lowering the migration or diffusion of corrosive ions to the metal surface, and increasing its electrical resistance [5].

Many medicinal substances and medication have been identified as possessing chemical characteristics like those of some CI [4, 26, 28, 29], since their chemical

structures are similar. This is because they contain electronegative atoms and functional groups that can facilitate their adsorption onto the metallic surface, and form an adherent protective surface film [5, 12, 16]. Medicines used as CI have relatively higher IE(%), as they possess complex molecular structures, with N, O and S multiple hetero-atoms and non-bonding π-electrons [12, 28, 30]. Most heterocyclic medicines, according to reports, are ecologically friendly [16]. The present work used MBZ as a chemical inhibitor of MS corrosion in a 0.5 M H_2SO_4 solution, using experimental and theoretical approaches. MBZ is a synthetic $C_7H_6N_2$ derivative. It is a white to yellowish powder that is soluble in formic acid and other inorganic acids, but not in water or most organic solvents. MBZ chemical formula is $C_{16}H_{13}N_3O_3$, and its molecular weight is 295.30 g/mol [30-33]. One of its most common pharmacological use is as an anthelmintic (worm-killing) agent [31]. MBZ is being experimentally and theoretically studied as a suitable corrosion inhibitor for MS in H_2SO_4 and similar acidic service environments, since it is a low cost, non-toxic and biodegradable compound, with O and N hetero atoms in its aromatic ring structure (Fig. 1).
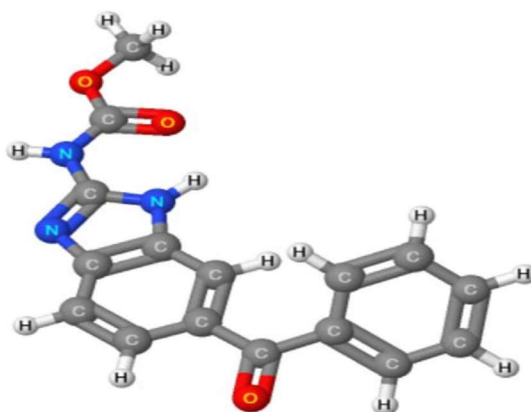

Figure 1: MBZ optimized 3D molecular structure [34, 35].

Experimental techniques
The following is a step-by-step summary of the experimental methodologies and procedures used in this study.

Materials reparation
Test media
All WL studies were carried out at room T in a 0.5 M H_2SO_4 solution made from double-distilled deionized water. The experiments were performed with 100 mL of the test media. A local pharmacy provided Wormin® MBZ (made by Cadila Pharmaceutical Ltd., Dholka, India).

Test specimen preparation
The chemical composition of a 16 mm cylindrical MS rod used for this examination was described in the authors' prior investigations [32, 33]. The rod was meticulously cut and sliced into several 15 x 10 mm long test coupons. For the specimens suspension, a 5 mm hole was drilled in their centre.

Before each experiment, MS samples were polished with numerous grades of emery paper (from 800 to 1200), and, afterwards, they were cleaned with distilled water and cleansed with acetone.

FTIR spectroscopy characterization of the inhibitor

Agilent Technologies' FTIR Cary 630 was used to assess MBZ functional properties. During the analysis, the inhibitor sample was scanned using transmittance method, and FTIR spectra were acquired over a wavenumber range from 650 to 4000 cm^{-1}, with a resolution of 8 cm^{-1}. MBZ chemical bond information and functional groups were detected using FTIR characterization.

WL measurements

MS test coupons were weighed and suspended in in 100 mL beakers containing the prepared test media, for 24, 48, 72, 96 and 120 h IT, with and without MBZ. They were removed when the required IT expired. The corrosion products were removed from MS samples by washing them in distilled water, rinsing in acetone and drying in ambient air. The coupons were then re-weighed to obtain their final weights. WL measurement findings are shown in Table 1. CR (mL/year) was calculated using Eq. 1.

$$CR = \frac{87.6 \times WL \times 1000 \, mg}{D \times A \times IT} \qquad (1)$$

where D is density (g/cm^2) and A is area (cm^2). IE(%) for MBZ was calculated using the relationship given in Eq. 2a.

$$IE(\%) = \frac{CRc - CRi}{CRc} \times 100 \qquad (2a)$$

CR$_c$ and CR$_i$ were determined without and with MBZ various C, respectively. IE(%) of MBZ was calculated for all its C during various IT of MS in H$_2$SO$_4$. θ by MBZ was determined using Eq. 2b.

$$\theta = \frac{CRc - CRi}{CRc} \qquad (2b)$$

Curves showing the relationship between IE(%) of MBZ, C and θ, and IT of MS, were also plotted.

Electrochemical measurements

IE(%) of MBZ was evaluated using a VersaSTAT 4 Electrochemical System auto lab potentiostat/galvanostat, controlled from a PC suitably equipped through a USB interface, and with Versa Studio electrochemistry software suite. All the experiments were conducted in a Pyrex glass cell with three electrodes. The WE was a test piece enclosed in polyester resin, with a total area of 1 cm^2 exposed to a corrosive liquid, and the CE was a Pt rod. The RE was an Ag/AgCl rod. These electrodes were connected to the electrolytic cell by a Luggin capillary. All the electrochemical test procedures and parameters were per the authors' previous investigations [32, 35], and their values are shown in Tables 2 and 3. IE(%) was calculated according to Eq. 3.

$$IE(\%) = \frac{icorr_c - icorr_i}{icorr_C} \times 100 \qquad (3)$$

where i_{corri} and i_{corrc} were determined for the MS coupon in the H_2SO_4 solution without and with MBZ, respectively, at a specified C.

SEM characterization of the MS surface

Following WL measurements, the corroded MS coupons surface morphology was scanned and examined by a SEM Phenom Pro X Model (Phenom world, Eindhoven, Netherlands) equipped with appropriate EDXS, for elemental and corrosion product characterization. The scanning techniques and SEM instrument parameters were reported in the authors' previous studies [32, 35, 36].

DFT studies

All quantum chemical investigations were carried out utilizing DFT/B3LYP methods with the 6–311 G (d, p) basis set, which is very reliable for geometrical optimizations, using the Gaussian 09 software. Because corrosion occurs in the aqueous phase, it is computationally appropriate to incorporate the solvent effect. Hence, all quantum computations were done in the aqueous phase, using SCRF theory and PCM. HOMO, and LUMO have been measured as quantum chemical characteristics linked to [37, 38] E_{LUMO}, E_{HOMO} and Δ. In an aqueous solution, μ and N110 were computed using Gaussian 09 W [39].

ΔN from MBZ molecules onto the MS surface, during inhibitor-metal interaction, was computed using Eq. 4.

$$\Delta N = \frac{\emptyset - \chi_{inh}}{2(\eta_{Fe} + \eta_{inh})} \qquad (4)$$

$\emptyset$ value was 4.82 eV, and Fe was 0 [40]. When ΔN is greater than zero, the metal electron transfer inhibition occurs, i.e., $\Delta N > 0$.

Fukui indices, which indicate the reactive centres within the molecules, may be used to analyse local reactivity [41].

MDS

Accelrys Inc.'s Materials Studio 6.0 [42] was used to run MD simulations in a simulation box with periodic boundary conditions. A 5 slab was utilized to cut the Fe crystal, which was imported and cleaved along the (110) plane. The smart minimizer system was used to reduce the Fe (110) surface energy, which alleviated it. The Fe (110) surface was extended to a (10) supercell, in order to provide a large surface for the inhibitor action. A vacuum slab was built with a thickness of zero. A supercell with the dimensions of a = 28.66 Å, b = 40.53 Å and c = 33.24 Å, comprising 250 H_2O, $20H_3O^+$, $10H_2SO_2$ and 1 MBZ molecule, was created based on molecules to sulfate proportion in 0.5 M H_2SO_4 [43]. The test was run in a simulation box (28.66, 40.53, 33.24 $Å^3$), at 303/333 K, NVT ensemble (constant no. of atoms, volume and T) and COMPASS force field [44], with a time step of 1 fs and a total simulation time of 500 ps.

$E_{interaction}$ and $E_{binding}$ determined using Eqs. (5) and (6) [45, 46] were employed to understand MBZ/Fe (110) interfaces in the simulation framework.

$$E_{interaction} = E_{total} - (E_{surface + solution} + E_{inhibitor}) \qquad (5)$$

$$E_{Binding} = -E_{interaction} \qquad (6)$$

where E_{total} is the entire system total energy, $E_{surface + solution}$ is the total energy of the Fe (110) surface and HCl without inhibitor, and $E_{inhibitor}$ is MBZ total energy.

Optimization of IE(%) and other corrosion properties using RSM

Researchers have attempted to describe and optimize CI factors, and anticipate their responses using experimental design software packages and approaches such as RSM [47-50]. IE(%) and other corrosion parameters were changed using RSM, based on the CCD tool of Design-Expert software version 11. A quadratic design model was employed in the investigation. WL, CR, IE(%) and θ were employed as response variables (1 to 4), while C and IT were employed as independent factors (1 and 2). To acquire the optimized responses of the dependent variables, a total of 30 tests runs was carried out.

Results and discussion

FTIR spectroscopy analysis
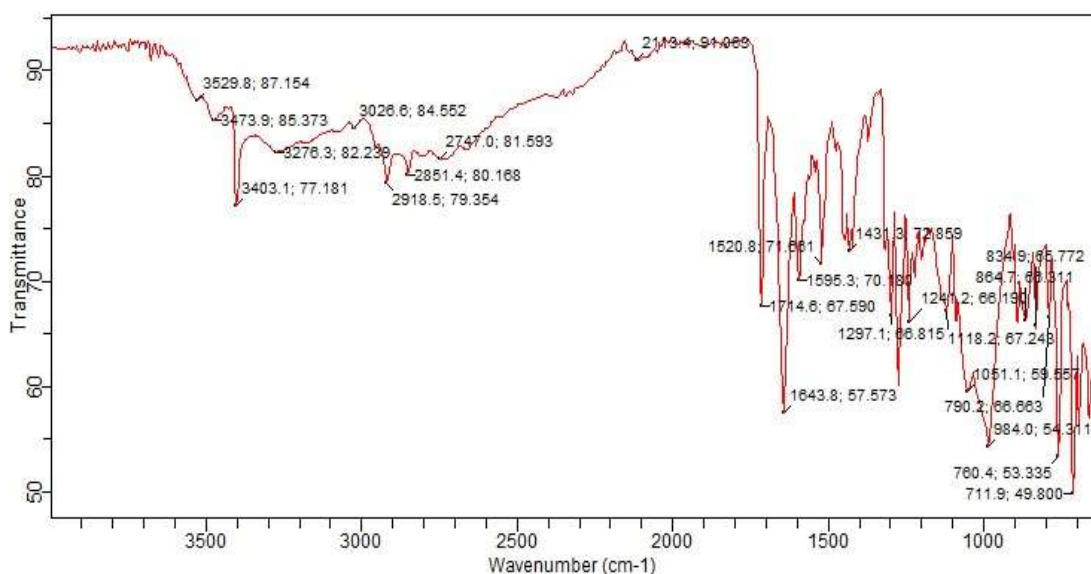
Fig. 2 illustrates FTIR spectra for MBZ.

Figure 2: FTIR spectra for MBZ.

CI and molecular adsorption of MBZ onto MS surfaces in H_2SO_4 were due to the functional groups and bond types within its structure. Inside MBZ molecular structure, due to NH group, there was a band from 3276 to 2113.4 cm^{-1}, which is associated with intense stretching of the imidazole ring [7, 51]. C=N group was in the ranges from 1743 to 1595 cm^{-1}. C=C group was in the ranges from 1431 to 1241 cm^{-1}. The bands from 1241 to 1051 cm^{-1} and from 984 to 711.9 cm^{-1} depict in-plane and out of plane CH bending deformation of the imidazole ring, respectively. CH$_3$ strong symmetric and asymmetric stretching bonds were also assigned from 3026.6 to 2918.5 cm^{-1} [52]. C-C ring stretching vibrations were observed at the frequency bands from 1643.8 to 1431.3 cm^{-1} in FTIR spectra.

Gravimetric measurements

Table 1 shows WL and CR of MS, and IE(%) for MBZ, whereas Figs. 3 to 10 show a graphical representation and comparison of the corrosion parameters.

At several C (0, 0.5, 1.0, 1.5, 2.0 and 2.5 g), IE(%) of MBZ against MS corrosion, in 0.5 M H_2SO_4, was investigated.

Table 1: CI results from WL of MS in 0.5 M H_2SO_4, at various IT, without and with MBZ, in various C.

IT (h)	MS and MBZ parameters	C of MBZ (g/L)					
		Blank	0.5	1.0	1.5	2.0	2.5
24	WL (g)	1.77	0.14	0.11	0.07	0.06	0.08
	CR (mm/yr)	1.31	0.10	0.08	0.05	0.04	0.06
	IE(%)	-	93.79	96.05	96.61	95.48	92.09
	θ	-	0.94	0.96	0.96	0.95	0.92
48	WL (g)	3.18	0.17	0.22	0.22	0.13	0.15
	CR (mm/yr)	1.18	0.06	0.08	0.08	0.05	0.06
	IE(%)	-	94.65	93.08	93.08	95.91	95.28
	θ	-	0.95	0.93	0.93	0.96	0.95
72	WL (g)	1.76	0.36	0.22	0.1	0.32	0.13
	CR (mm/yr)	0.43	0.09	0.05	0.02	0.08	0.03
	IE(%)	-	87.5	94.32	81.82	92.61	79.55
	θ	-	0.88	0.94	0.82	0.93	0.80
96	WL (g)	2.11	0.5	0.45	0.28	0.38	0.31
	CR (mm/yr)	0.39	0.09	0.08	0.05	0.07	0.06
	IE(%)	-	78.67	86.73	81.99	85.31	76.30
	θ	-	0.79	0.87	0.82	0.85	0.76
120	WL (g)	3.74	0.41	0.35	0.32	0.48	0.35
	CR (mm/yr)	0.55	0.06	0.05	0.05	0.07	0.05
	IE(%)	-	90.64	91.44	87.17	90.64	89.04
	θ	-	0.91	0.91	0.87	0.91	0.89

WL (g), CR (mm/yr), IE(%) (76.303-96.610%) and θ (0.76303-0.96610) ranges showed that MBZ effectively protected MS in H_2SO_4. This was due to MBZ molecules and atoms adsorption onto the MS test coupons surface, which formed a surface barrier coating against H_2SO_4. MS low CR and WL values obtained by gravimetric measurements (Fig. 1) was due to IE(%) and θ relatively high values for MBZ, because of its ringed structure with N and O heteroatoms, and non-bonding π-electrons [30, 53]. These hetero-atoms and free-electron sites enabled MBZ adsorption onto the MS surface, providing it with enough corrosion resistance.

CR values of MS in 0.5 M H_2SO_4 were substantially reduced with its higher IT and C of MBZ, due to the inhibitor molecules action on the alloy surface (Figs. 3 and 4). CR was the lowest (0.024667 mm/yr), after 72 h IT of MS in the H_2SO_4 solution with 1.5 g/L MBZ. MBZ highest IE(%)was 96.610% for MS in 1.5 g/L H_2SO_4, with 24 h IT. MBZ was particularly successful as CI on MS in 0.5 M diluted H_2SO_4, as proven by the fact that CR and WL of the latter were much lower in the solution with the former than in the one without it.
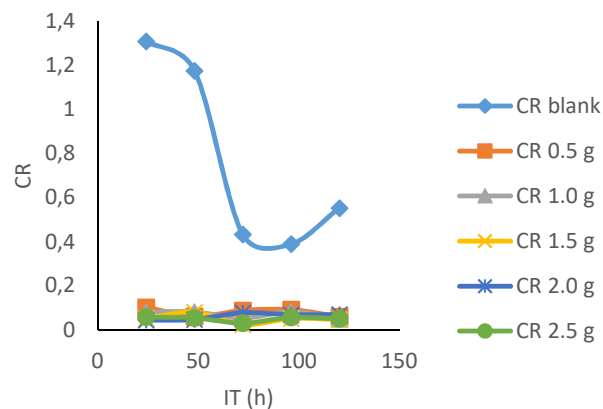
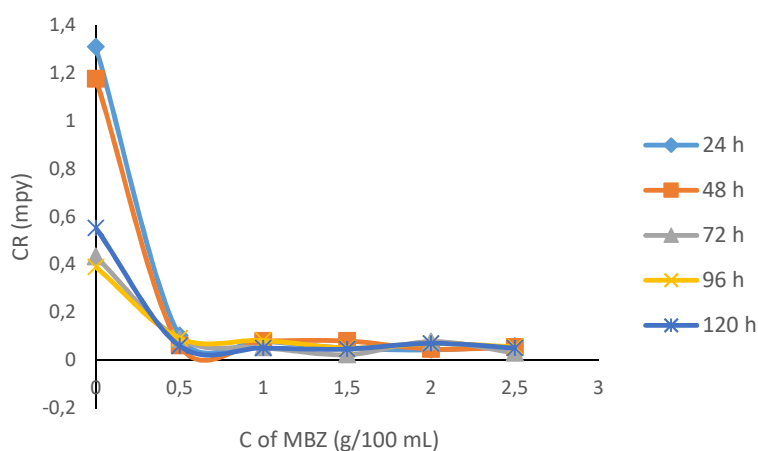**Figure 3:** CR of MS in HCl for different IT at various C of MBZ.

Figure 4: Variation in CR (mm/yr) for MS with C of MBZ.

WL (Fig. 5), for MS in 0.5 M H_2SO_4 without and with MBZ, in varying C, was remarkably reduced when the latter was added to the corrosive solution. On a close inspection, WL of MS decreased to a maximum, with higher C of MBZ, and longer IT, before maintaining a near-constant value, and then it slight increased. The test without MBZ recorded the highest WL and CR values for MS during its IT.
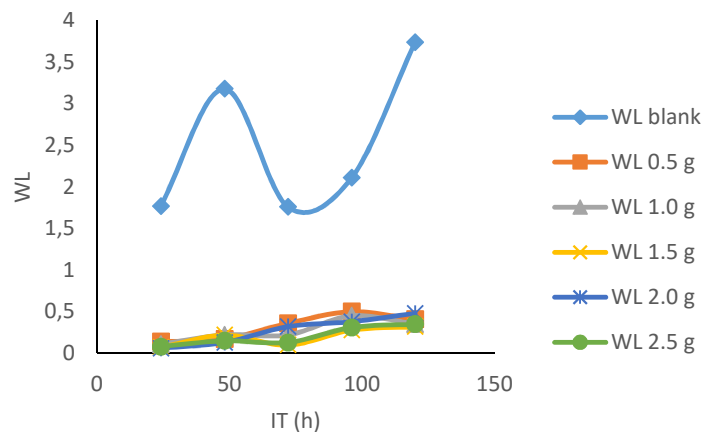

Figure 5: Dependence from WL of MS on IT.

Fig. 6 revealed a marked reduction in WL, as C of MBZ was increased from 0 to 2.5 g/L, for all the considered IT. MBZ successfully decreased the CR of MS in H_2SO_4 to a minimal level. The plots of CR, IE(%) and θ against IT and C, as shown in Figs. 3, 4, 7-10, revealed a similar trend.
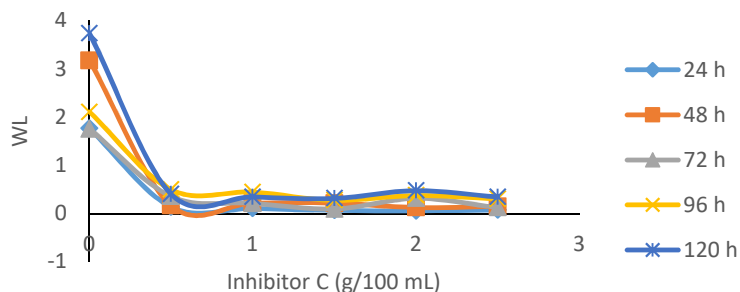

Figure 6: Dependence from WL of MS on C of MBZ.

Fig. 7 shows that IE(%) decreased with higher IT, but remained above 70% for all IT, and increased with growing C of MBZ (Fig. 8).
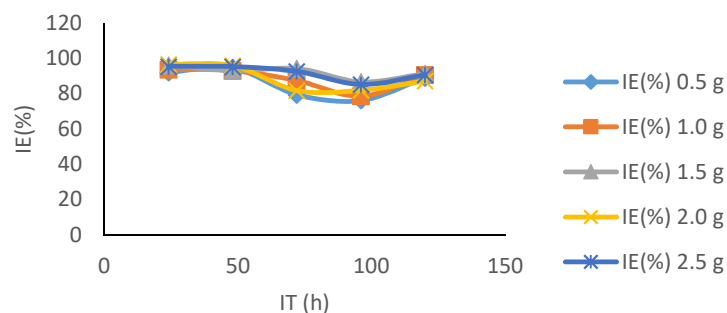

Figure 7: Effect of IT for MS in 0.5 M H_2SO_4 on its corrosion IE(%) by different C of MBZ.
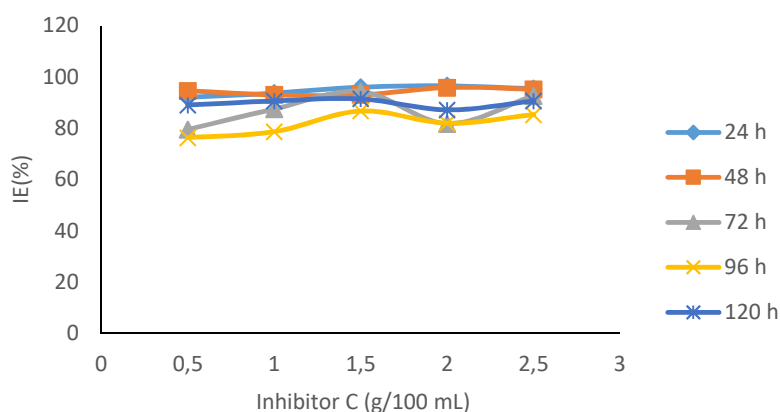

Figure 8: Dependence from CI of MS by MBZ on its C, for various IT in 0.5 M H_2SO_4.

Figs. 9 and 10 show that MBZ protective thin film provided enough coverage of the MS surface in H_2SO_4, throughout the IT, significantly reducing active corrosion sites.
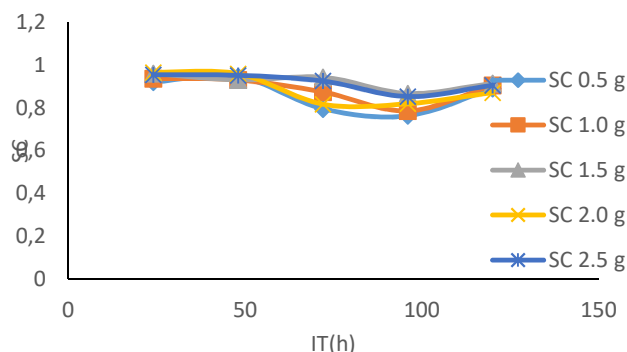
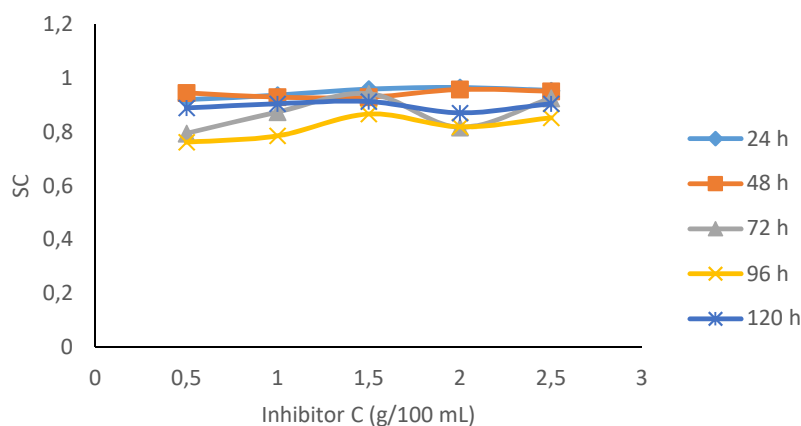**Figure 9:** Dependence from θ by MBZ on the IT of MS in 0.5 M H_2SO_4.

Figure 10: θ variation with different C of MBZ.

Electrochemical measurements

PDP measurements

Fe anodic breakdown to Fe^{2+} is thought to be the cause of MS corrosion in aggressive acidic environments [54-56]. Using Tafel extrapolation/polarization measurements, the effect of MBZ various doses on MS anodic dissolution, and on the related cathodic reduction of H ions during the corrosion process, was determined. MBZ addition to the H_2SO_4 solution moderately changed anodic and cathodic half-reactions, as seen by Tafel plots in Figs. 11 and 12.
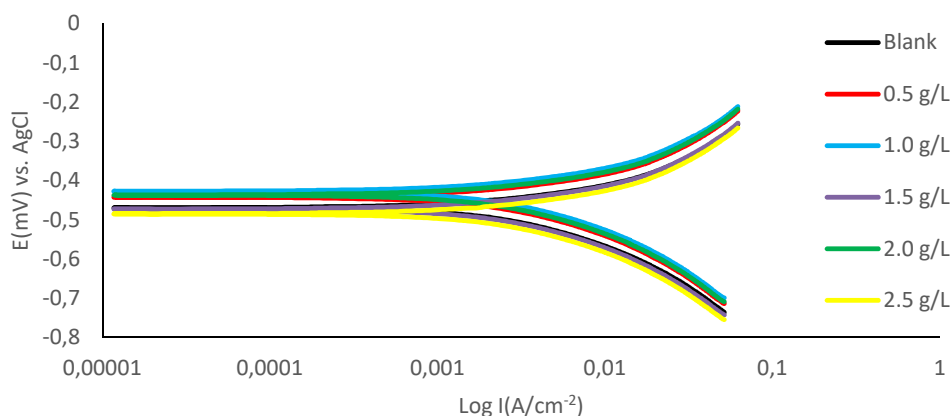

Figure 11: PDP curves for MS in 0.5 M H_2SO_4 without and with MBZ, in various C, at 303 K.
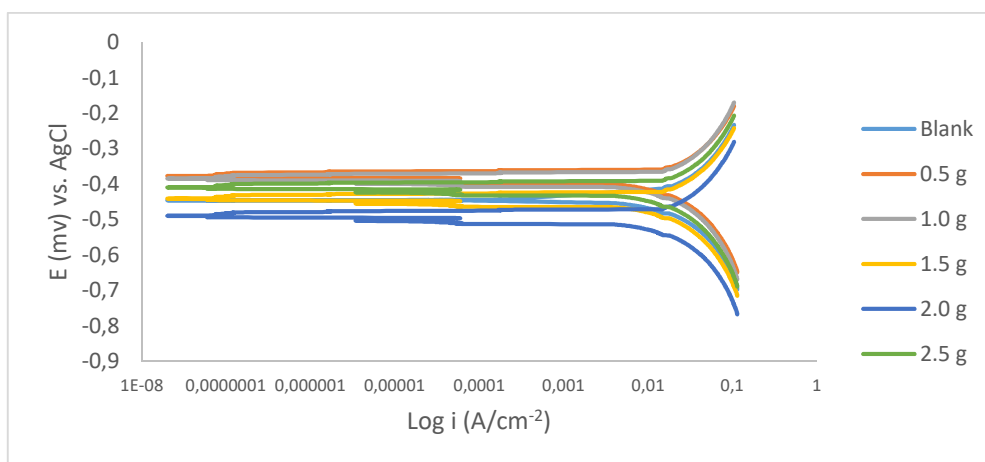
Figure 12: PDP curves for MS in 0.5 M H_2SO_4 without and with MBZ, in various C, at 333 K.

Tafel curves extrapolation yielded PDP values shown in Tables 2 and 3. MBZ addition resulted in E_{corr} huge displacement, as it can be seen in the tables. For all C of MBZ, anodic and cathodic Tafel constants were available. This suggests that MBZ is a mixed-type inhibitor. According to the overall polarization data, the trial without MBZ exhibited the highest CR. PDP test revealed that MBZ had a significant impact on the electrochemical process that led to the corrosion reaction. In addition, differences in the cathodic and anodic Tafel constants between the H_2SO_4 solution without and with MBZ indicate that redox reactions connected with the corrodent were impeded by the thin film formed by the inhibitor [18].

The development of an adherent protective coating, and MBZ adsorption onto the MS surface, can be linked to the inhibitor corrosion IE(%) [18, 35, 57, 58]. I_{corr} values for the tests with MBZ and without it reinforce this conclusion (Tables 2 and 3). Since E_{corr} displacement obtained in the test without MBZ (Tables 2 and 3) was less than 85 mV, at 303 and 333 K, it was deduced that it functioned as a mixed-type inhibitor, based on PDP data [30, 59].

Table 2: PDP values for MS in 0.5 M H_2SO_4 without and with MBZ, in various C, at 303 K.

MBZ C (g/L)	I_{corr} (mA)	E_{corr} (mV)	CR (mm/yr)	IE(%)	β_a (mV)	β_c (mV)
0.0	-3.352	-470.939	24.779	-	198.367	123.246
0.5	-179.323	-442.306	1.3254	94.651	130.587	89.324
1.0	-103.823	-437.697	0.76734	96.903	121.614	67.34
1.5	-155.868	-452.045	1.152	95.351	122.923	80.257
2.0	-136.153	-437.823	1.0063	95.939	131.168	76.031
2.5	-138.462	-464.284	1.0234	95.870	124.738	91.449

Table 3: PDP values for MS in 0.5 M H_2SO_4 without and with MBZ, in various C, at 333 K.

C of MBZ (g/L)	I_{corr} (mA)	E_{corr} (mV)	CR (mm/yr)	IE(%)	β_a (mV)	β_c (mV)
0.0	-34.01	-440.497	251.37	-	400.406	351.646
0.5	-12.06	-396.102	89.136	64.540	317.637	173.616
1.0	-563.79nA	-422.048	0.0041669	99.998	83.216	129.55
1.5	-1.765	-422.933	13.049	94.809	173.434	78.959
2.0	-1.66	-430.981	12.274	95.117	185.951	89.983
2.5	-1.876	-419.401	13.867	94.483	214.317	67.60

Furthermore, H_2SO_4 solutions with MBZ had lower i_{corr} values than those of the blank ones. MBZ addition reduced cathodic and anodic half-reactions, thus supporting also the inference that it is a mixed type inhibitor [30, 36].

At 303 and 333 K, corrosion IE(%) obtained using PDP parameters was slightly higher than that calculated using WL data. At 303 K, 1.0 g MBZ inhibited MS corrosion in H_2SO_4, with a maximum IE(%) of 99.998%. At 303 K, 1.0 g MBZ gave a maximum IE(%) of 96.903%. The similarity in the corrosion IE(%) values obtained at ambient T, by both gravimetric and PDP techniques, suggest agreement of both methods.

T effect

At 303 and 333 K, T effect on CR and IE(%) was investigated. As a rule of thumb, the rate of a chemical reaction doubles at every 283.15 K increase in T; so, corrosion kinetics, as an electrochemical process, should increase as T rises [32]. With MBZ, a modest decrease in IE(%) and an increase in CR were detected at higher T, implying the creation of a physical/electrostatic adsorption coating [60, 61]. On the other hand, chemisorption occurs when there is an increase in IE(%), a drop in CR with higher T, lower acid C, and decreased E_a rate [60, 61].

MBZ lower IE(%) and MS higher CR observed in 0.5 M H_2SO_4 with low inhibitor C, at 333 K, revealed that the critical C of anions required for metals and alloys corrosion protection rose with higher T and aggressive solutions C [53, 60, 62].

Analysis of adsorption isotherms

The concept of molecular adsorption can be used to further explain CI mechanisms, as it is generally affected by the inhibitor chemical structures, the charge distribution in the molecule, the metal nature and surface charge, and the type of corrosion media [18, 61]. Evaluation of experimental data obtained with multiple adsorption isotherms is used to determine the most likely method of adsorption. Frumkin's, Temkin's, Freundlich's and Langmuir's isotherms are the most commonly used adsorption models for researching the inhibition mechanism of the corrosion process. Based on the given mathematical relations, K_{ads} and G°_{ads} values were calculated (Eqs. 7 and 8). The adsorption isotherms characterize the inhibitor molecules interactions with the active corrosion sites on the metal surface [5], and give more information on the CI mechanism. In this study, Temkin's and Langmuir's adsorption isotherms were investigated to determine MBZ adsorption mechanism onto the MS surface. With a linear graph, near unity slopes (1.0423 and 0.969) and R_2 values of 0.9999 and 0.9839, at 303 and 333 K, Langmuir's adsorption isotherm provided the best and most suitable description of MBZ behaviour, confirming its constituents adsorption onto the corroding MS surface. The interactions of the adsorbate species with the MS surface, as well as variations in Q_{ads} with increasing θ, can be attributed to the modest departure of the slopes and R_2 of the Langmuir's plot from unity [63]. The linear form of the Langmuir's adsorption isotherm given in Eq. 7 was used to plot the adsorption isotherm provided in Fig. 13.

$$\frac{C_{inh}}{\theta} = \frac{1}{K_{ads}} + C_{in} \tag{7}$$

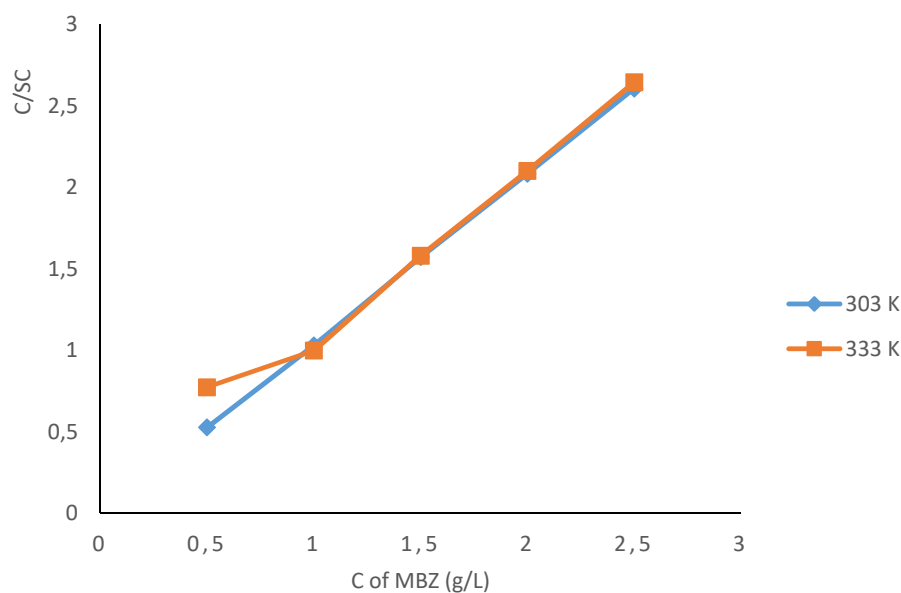**Figure 13:** Langmuir's adsorption isotherms for MS in 0.5 M H_2SO_4 with various C of MBZ, at 303 and 333 K.

The change in ΔG°_{ads} was obtained using Eq. 8:

$$\Delta G^\circ_{ads} = -RTln(55.5K_{ads}) \tag{8}$$

where R is the universal gas constant (8.314 kJ^{-1}/mol^{-1}) and 55.5 is the molar C (mol/L^{-1}) of water in the solution. K_{ads} and ΔG°_{ads} values were obtained at various T and MBZ C (Table 5). High K_{ads} and negative ΔG°_{ads} values were obtained for MBZ molecules, which implies their effective and spontaneous adsorption onto the MS surface in 0.5 M H_2SO_4. ΔG°_{ads} magnitude is a decisive factor in the adsorption process. Physisorption is generally associated with ΔG°_{ads} values around -20 kJ·mol^{-1} and below, while chemisorption is attributed to ΔG°_{ads} values around -40 kJ·mol^{-1} and above [5, 7, 9, 32, 35]. ΔG°_{ads} estimated values for MBZ varied from -15.4720 to -18.7870 and from -14.6965 to -18.0345 kJ/mol$^-$, at 303 and 333 K, respectively, as shown in Table 4.

Table 4: ΔG°_{ads}, θ and K_{ads} calculated for MBZ in 0.5 M H_2SO_4.

T (K)	MBZ C (g/L)	ΔG°_{ads} (kJ/mol^{-1})	K_{ads} (mol^{-1})	θ
	0.5	-18.7870	35.3902	0.94651
	1.0	-18.4818	31.2893	0.96903
303	1.5	-16.4303	13.6703	0.95350
	2.0	-16.0665	11.8037	0.95939
	2.5	-15.4720	9.2852	0.95870
	0.5	-14.6965	3.6402	0.64540
	1.0	-15.5749	4.9990	0.99998
333	1.5	-18.0345	12.1538	0.94809
	2.0	-17.4214	9.7396	0.95117
	2.5	-16.4471	6.8503	0.94483

This indicates that MBZ adsorption process was physisorption. As T and C of MBZ were increased from 303 to 333 K and from 0.5 to 2.5 g/L, respectively, $\Delta G°_{ads}$ and K_{ads} values decreased; a similar pattern was described in the literature [27, 32].

SEM analysis

Figs. 14a and b show micro-analytical pictures of MS specimens before and after corrosion, with and without MBZ.
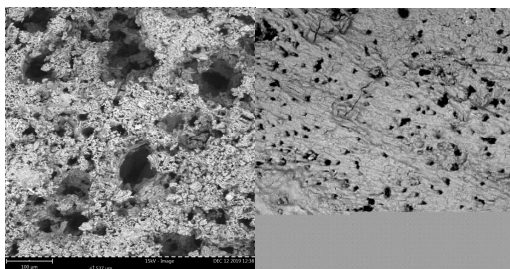

Figure 14: SEM surface morphology of MS specimens after gravimetric experiments in H_2SO_4: **(a)** without MBZ and **(b)** with MBZ.

The blank H_2SO_4 solution corroded the MS surface (Fig. 14a), which has a significantly deteriorated morphology, with obvious and deep macro and micro pits. Due to MBZ corrosion IE(%)on MS, Fig. 14b depicts a transition to a relatively smooth surface shape.

DFT studies

DFT-based structural analysis can be used to assess $C_7H_6N_2$ carbamate MBZ derivative reactivity. Δ, E_{HOMO}, E_{LUMO} and N110 are considered good overall indices for assessing MBZ IE(%) of MS surfaces corrosion [64]. In acidic media, protons are assumed to be present, making the protonation of organic molecules more likely. The most critical protonation site is displayed in Fig. 15, and MBZ had no active protonation site in acidic Ph, for fixing H+ to a pH of 3.42.
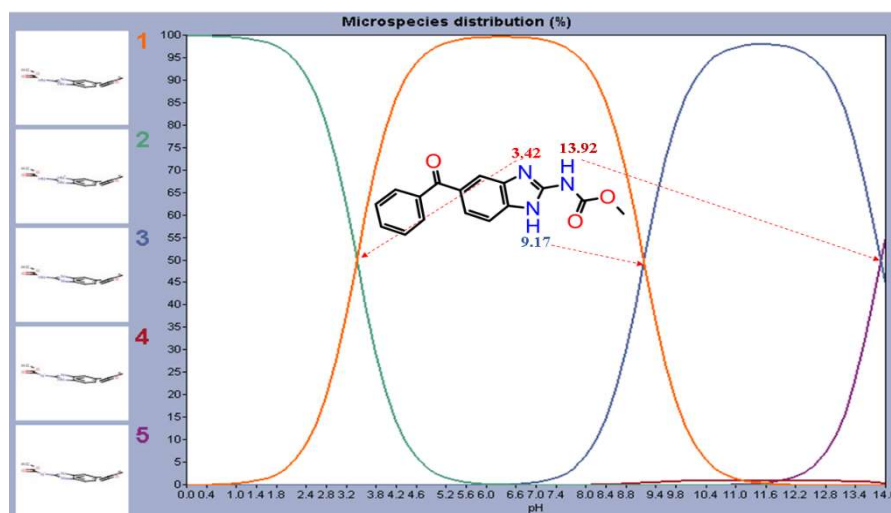

Figure 15: Possible MBZ molecules forms by varying pH from 0 to 14.

Thus, it was assumed that the molecule was stable at the acidic pH used in this experiment, as assessed by Marvin View software. At an acidic pH (pH$_{exp}$ of 0.5 M H$_2$SO$_4$ is pH = -log(0.5) = 0.301), MBZ had no protonation state, which means that the only neutral form remained in the solution. This is beneficial, because several experiments have shown that the protonation form of the molecule is not absorbed.

MBZ molecule optimal configurations and molecular electrostatic E distribution are shown in Fig. 16. The most stable and energy-efficient systems are interconnected systems. The average density (red colour) of MEP distribution is centred on O atoms of carbonyl groups; O8 atom has several electrons in this circumstance, facilitating the sharing phenomenon with the vacant iron orbitals [65].
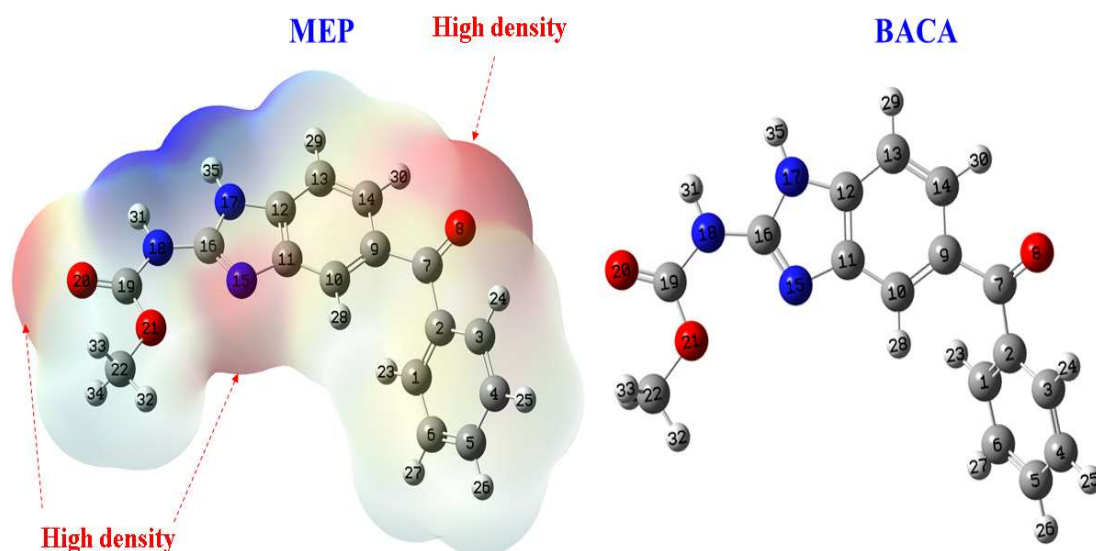

Figure 16: MBZ optimized frameworks and MEP distribution.

The distribution of electron density in molecular frontier orbitals (HOMO and LUMO) is described as global reactivity, as seen in Fig. 17, where HOMO electron density can be found on any chemical surface, except on the phenyl group linked to the carbonyl function. This demonstrates that MBZ contains a large number of active electron donor sites throughout the skeleton. LUMO electron density is represented over a wide section of the compound surface, except for the phenyl group, implying considerable adsorption of this substance onto the metal surface. E$_{HOMO}$ high value (-5.4754 eV) for MBZ indicates that it can effectively exchange electrons with empty spaces on the metal surface. This means that MBZ-metal is highly reactive. MBZ positive value of ΔN, but less than 3.6 (Table 5), means that it can release and share its electrons [66-68]. O (O8 and O20) and C$_7$H$_6$N$_2$ ring electron cloud are the active centres in MBZ, and they are responsible for this electron sharing behaviour. The μ descriptor interprets the polarizability of the chemical compounds under investigation; high polarizability (reactivity), i.e. strong adsorption of the inhibitory molecule onto the metallic surface, is shown by a high value of this descriptor [69].
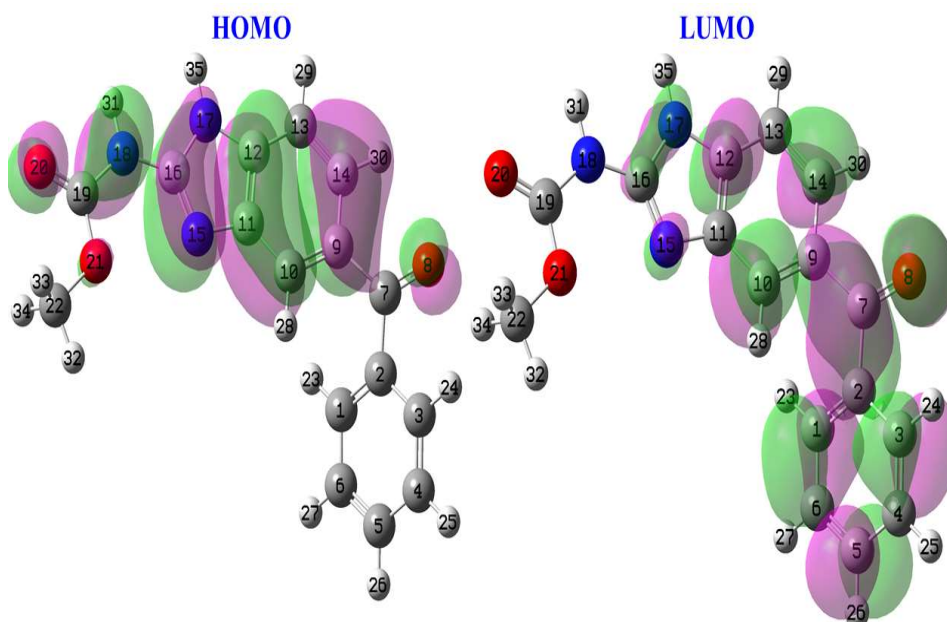
Figure 17: FMO distributions for MBZ.

Local reactivity is a popular strategy for determining the local active areas of a chemical inhibitor [70].

Tables 5 and 6 show the chemical structure descriptors and calculated Fukui indices of simplified functions (f+ and f-) for MBZ, respectively.

Table 5: Descriptors of MBZ molecule chemical structure.

Complex	E_{LUMO}	E_{HOMO}	μ	Δ	ΔN
MBZ-Fe	-2.1135	-5.4754	4.9782	3,3619	2.5744

Table 6: Fukui indices for MBZ f^+_k and f^-_k measured at DFT/GGA/DNP.

Atom	f^+_k	f^-_k	Atom	f^+_k	f^-_k
1 C	0.16820	-0.12004	12 C	-0.15573	0.22856
2 C	-0.13104	0.11047	13 C	0.16297	-0.09522
3 C	0.13203	-0.06242	14 C	0.21594	-0.07532
4 C	0.08012	-0.06134	15 C	0.34829	-0.19004
5 C	0.08959	-0.01851	16 C	-0.18038	0.28582
6 C	0.09187	-0.06577	17 C	0.46978	-0.47136
7 C	0.07746	0.08726	18 N	0.27686	-0.22970
8 O	0.03460	0.11203	19 C	-0.02668	0.06965
9 C	-0.10926	0.08992	20 O	0.06293	0.00204
10 C	0.32256	-0.18432	21 O	-0.00853	0.01471
11 C	-0.13117	0.12038	22 C	0.31706	-0.31829

Fig. 18 shows the condensed atom Fukui functions, while Tables 5 and 6 show the chemical structure descriptors and calculated Fukui indices of simplified functions (f+ and f-) for MBZ. Atoms with higher f- and f+ values are electrophilic and nucleophilic active centres, respectively [71]. The findings show that O(8) atom underwent electrophilic assaults, indicating that it was prone to supply electrons, forming more stable coordination bonds with the metal surface. During nucleophilic assaults, atoms like C(10), C(12) and C(16) will accept electrons from the metal surface.
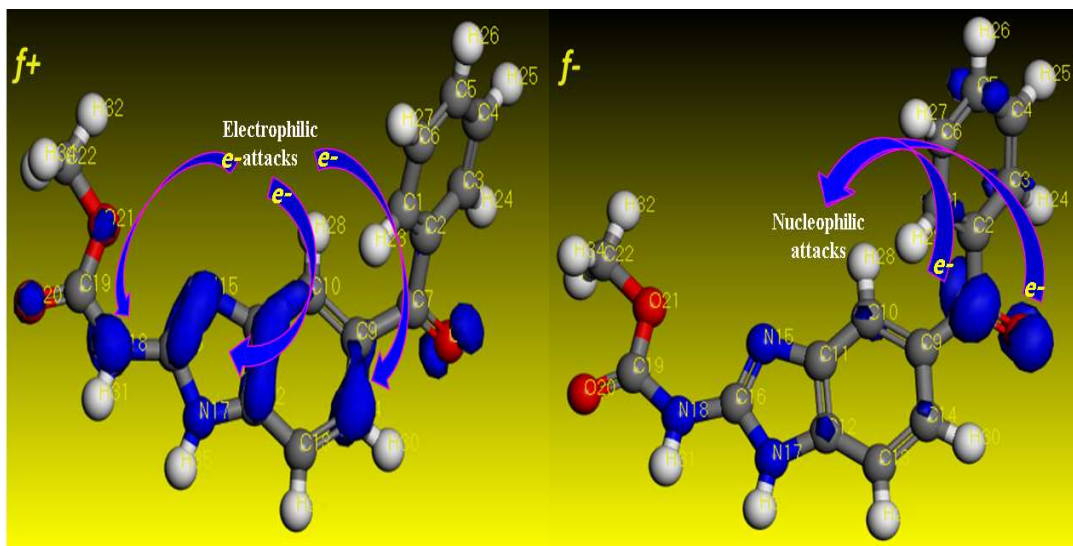
Figure 18: MBZ atom-condensed Fukui functions for f^+_k and f^-_k estimated at DFT/GGA/DNP, using Material studio software.

Electronic conduct of Fe-MBZ complex

Fe-MBZ complex was investigated using DFT method, to see how the metal surface affected the inhibitor electron density distribution and quantum chemical descriptors. The chemical quantum computing was done with the Gaussian 09 software, and DFT was done on the B3LYP/LanL2DZ level. Fig. 19 shows Fe-frontier-molecular MBZ orbitals, optimized structure and electronic density distribution.
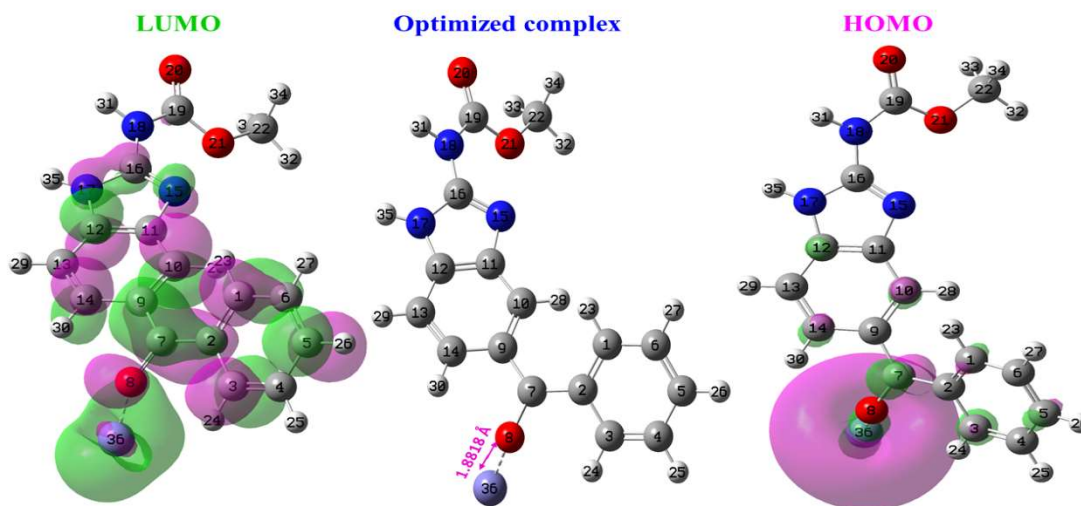
Figure 19: Fe-MBZ complex FMO distributions and MBZ Fe-O(11) distance.

There was no visible change in spatial conformation for MBZ optimized structure coupled to the Fe atom, when compared to its structure alone. As a result, Fe and O atoms are at the core of HOMO mass (O8). HOMO high density on the Fe atom indicates that it has received electrons from the inhibitor, resulting in a decrease in MBZ electronic density. LUMO, on the other hand, is almost on the complex

structure. Therefore, the result for MBZ alone is the same. Hence, MBZ electron donor property to Fe atom was improved. Table 7 groups key quantum chemical descriptors values. Fe iron atom had a favourable impact on overall chemical reactivity, according to the results in this table. A drop in Δ and an increase in ΔN and μ values demonstrated this. These findings show that MBZ and Fe surface communicated effectively.

Table 7: Chemical structural descriptors for Fe-MBZ complex.

Complex	E_{HOMO}	E_{LUMO}	μ	Δ	ΔN
MBZ-Fe	-3.5793	-1.3926	11.4998	2.1866	1.06739

MD modeling

When the adsorption mechanism at the MBZ-metal interface was studied, theoretical modelling methods concentrated on MD simulation [72]. When the inhibitor adsorbed onto the adsorbate, the fluctuation energies and T curves (303 and 333 K) were in equilibrium, as shown in Figs. 20 and 21, which illustrate top and lateral views of MBZ adsorption configurations on MS surface in H_2SO_4, at 303 and 333 K.

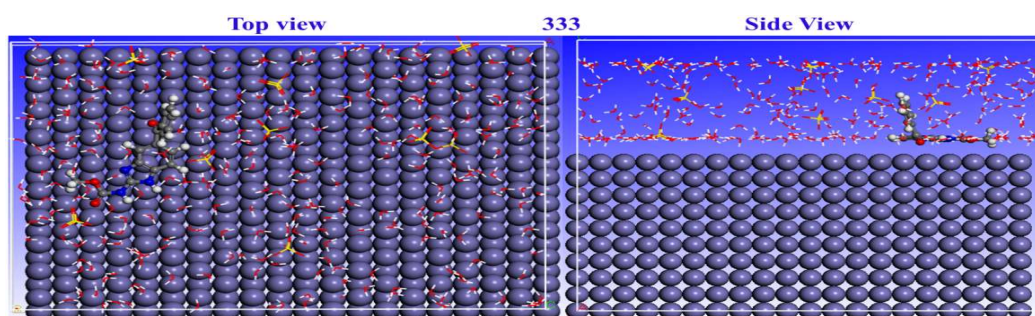**Figure 20:** MD structures of MBZ adsorption onto the Fe(1 1 0) surface, at 303 K.
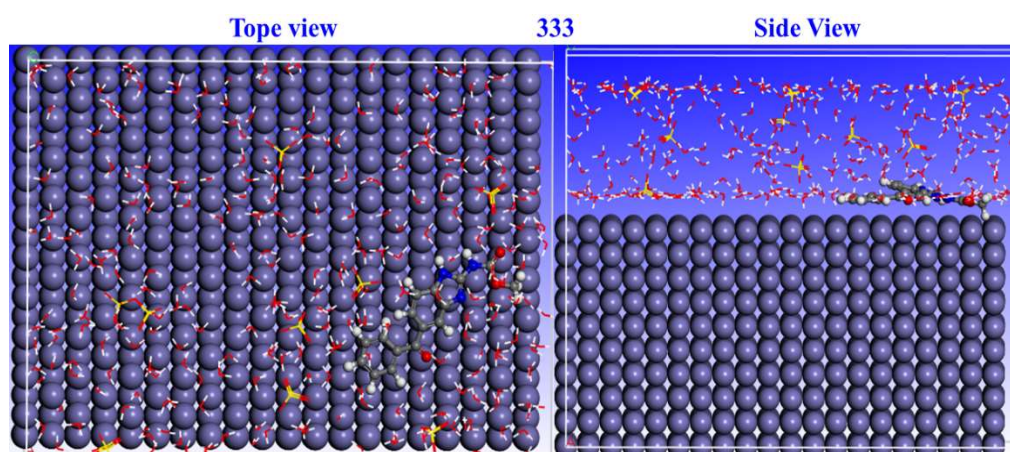

Figure 21: MD structures of MBZ adsorption onto the Fe(1 1 0) surface, at 333 K.

MBZ structure is visible on the initial Fe surface, indicating that the inhibitor molecule was firmly adsorbed. This could be due to the presence of covalent bonds at the MBZ-Fe (1 1 0) contact, which positively modified the adsorption behaviour.

This technique maximized θ qualities, by adsorbing the $C_7H_6N_2$ derivative. Indeed, this species is a powerful CI, confirming IE(%) findings of the experimental studies. Energy concepts, explicitly, $E_{binding}$ and $E_{interaction}$, were used to express the simulation findings. The magnitude of MBZ adsorption and contact with the MS surface was determined by the values of these terms. Negative touch energy projections confirmed MBZ-metal contact capabilities [73]. At 303 and 333 K, corresponding $E_{interaction}$ values for MBZ were -536.33 and -694.53 kcal/mol, respectively.

Results of optimization by RSM

WL, CR, IE(%)and θ were all affected by inhibitor C and IT, according to the results of optimization research. Figs. 22, 23 and 24 illustrate MBZ IE(%) on MS in 0.5 M H_2SO_4. Fig. 22 shows a linear graph of anticipated versus real IE(%), suggesting that the design model was adequate for predicting MBZ inhibition [50].
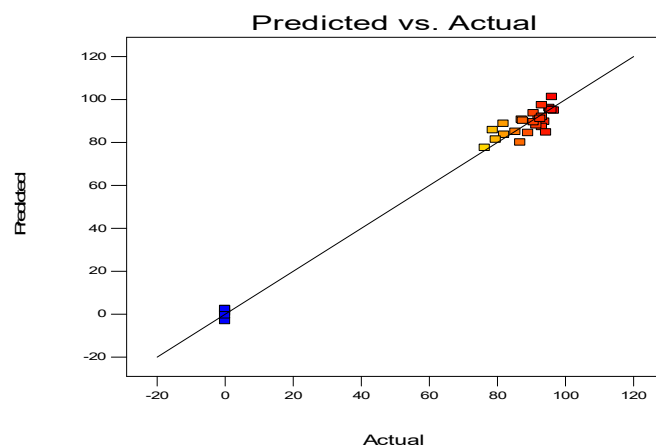

Figure 22: Diagnostic plot of predicted versus actual IE(%).

IE(%) level of reliance for MBZ C and IT was demonstrated by the 3-D surface plot (Fig. 23).
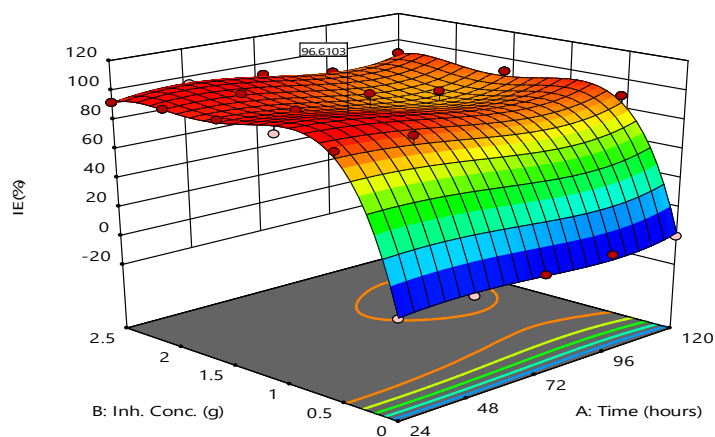

Figure 23: 3-D surface plot for IE(%) with the predicted value.

3-D surfaces structure suggests that, throughout the CI process, there were considerable interactions between the evaluated factors and the response variables. Fig. 24 shows a perturbation plot that can be used to compare the effects of various parameters on IE(%), at different points in the design space. Only one element changed over the response range, while the other remained constant. For all factors, the reference point was set by default to the midpoint (coded 0). This can be altered to any desirable point (perhaps the optimal run conditions). A component with a steep slope or curve implies that it is sensitive to the response. The response variable is insensitive to changes in that particular component, if the line is reasonably flat. The perturbation plot demonstrates the element that has the most impact on the response. IE(%) of MBZ was more responsive to its C (B) than to IT (A), in this case.
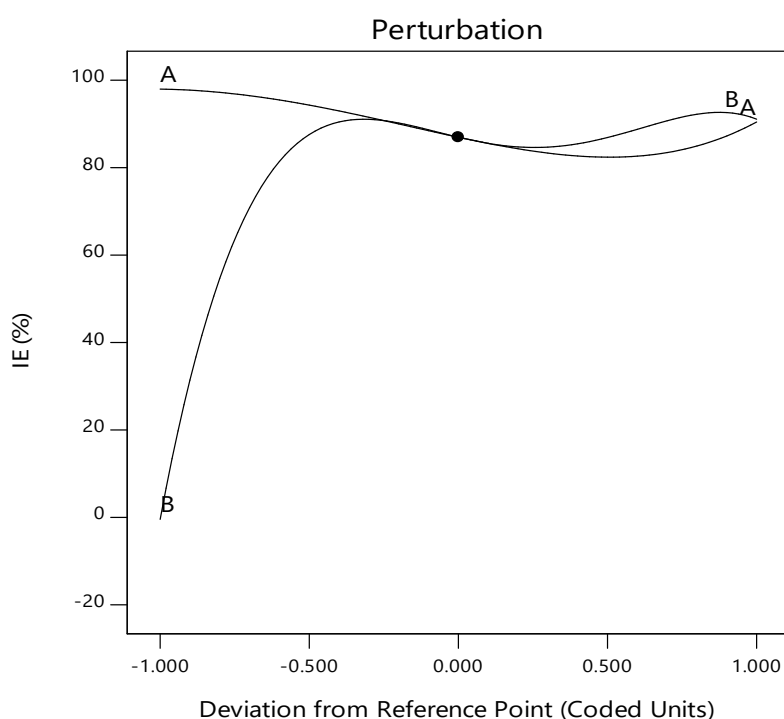
Figure 24: Perturbation curve showing the most influential factor.

Eq. 9 provides a predictive model Eq. of MBZ IE(%), as a function of the components evaluated in terms of factors coding. The quartic model Eq. represented the link between IE(%) and independent parameters, such as MBZ C (B) and IT (A). For given levels of each factor, the model Eq. written in terms of factor coding can be used to predict the response of the dependent variable. By default, the high values of the components are recorded as +1, while the low levels are coded as -1. By comparing the factors coefficients, the relative impacts of the elements can be determined using the coded Eq. [50].

$$IE(\%) = +86.96 - 14.62A - 16.17B - 1.35AB + 5.04A^2 + 15.36B^2 - 1.24A^2B + 3.57AB^2 + 10.87A^3 + 61.93B^3 - 6.37A^2B^2 + 2.32A^3B - 1.98AB^3 + 2.21A^4 - 56.99B^4 \qquad (9)$$

Table 8 contains a summary of the design parameters. F-value of 83.80 suggests a significant model, according to ANOVA results in Table 9. Due to noise, such high

Tables 8: Design summary for factor and response variables.

Factor	Name	Units	Type	Subtype	Min	Max	Coded	Values		Mean	SD
A	Time	h	Numeric	Continuous	24	120	-1.000 = 24	1.000 =120		72	34.5214
B	MBZ C	g	Numeric	Continuous	0	2.5	-1.000 = 0	1.000 =2.5		1.25	0.86851

Response	Name	Units	Obs	Analysis	Minimum	Max	Mean	SD	Ratio	Trans	Model
R1	WL	g	30	Polynomial	0.06	3.74	0.629	0.927542	62.3333	None	Quadratic
R2	CR	mm/yr	30	Polynomial	0.0246673	1.30984	0.181695	0.314399	53.1	None	Quartic
R3	IE	%	30	Polynomial	0	96.6102	74.6061	34.363	N/A	None	Quartic
R4	SC		30	Polynomial	0	0.966102	0.746061	0.34363	N/A	None	Quartic

Table 9: Response parameter (IE(%)) ANOVA results.

	Squares sum	Df	Mean square	F value	p-value prob > F
Source model	33811.45	14	2415.10	83.80	< 0.0001 signif.
A - time	308.56	1	308.56	10.71	0.0051
B - BMZ C	392.76	1	392.76	13.63	0.0022
AB	0.80	1	0.80	0.028	0.8695
A^2	3.73	1	3.73	0.13	0.7241
B^2	48.33	1	48.33	1.68	0.2149
A^2B	3.79	1	3.79	0.13	0.7218
AB^2	30.50	1	30.50	1.06	0.3199
A^3	159.38	1	159.38	5.53	0.0328
B^3	5090.45	1	5090.45	176.64	< 0.0001
A^2B^2	33.95	1	33.95	1.18	0.2949
A^3B	3.40	1	3.40	0.12	0.7360
AB^3	2.61	1	2.61	0.091	0.7676
A^4	0.95	1	0.95	0.033	0.8586
B^4	875.86	1	875.86	30.39	< 0.0001
Residual	432.28	15	28.82		
Cor total	34243.73	29	R-squared	0.9874	
SD	5.37		Adj R-squared	0.9756	
Mean	74.61		Pred R-squared	0.9506	
CV%	7.20		Adeq precision	27.497	
Press	1692.62		BIC	216.19	
-2 log likelihood	165.17		AIC	229.46	

F-value has a 0.01% probability of occurring. Model terms that have a value of prob > F less than 0.0500 are considered significant. A, B, A^3, B^3 and B^4 are the model significant terms in this example. Insignificant model terms are indicated by values greater than 0.1000. Since the difference is smaller than 0.2, pred. R-squared of 0.9506 is in reasonable agreement with adj. R-squared of 0.9756. These values are quite close to unity, indicating that the model was well-fit [74]. The signal-to-noise ratio is measured using adeq. precision. A signal-to-noise ratio of more than 4 is always preferable. The research yielded a signal-to-noise ratio of 27.497, indicating that the signal was strong, and that this model may be utilized to navigate the design space effectively.

Numerical optimization result
Table 10 presents the optimal solutions found to suitably satisfy the target optimization goals set for the factors and the responses after numerical optimization.

The optimization report reveals that a minimum inhibitor C of 1.061 g/L was required, for 48 h IT, in order to obtain an optimal IE(%) of 96.61%, with near-unity desirability (0.879).

Table 10: Numerical optimization report.

Time	MBZ C	WL	CR	IE(%)	θ	Desirability
48.581	1.061	0.060	0.084	96.610	0.922	0.879

Conclusions

WL measurements, PDP techniques, design optimization, DFT and MD modelling were used to study MS corrosion and its inhibition in 0.5 M H_2SO_4. Based on the analysis and interpretation of the findings, the study concluded that:

- According to the findings of the Tafel polarization investigation, MBZ acted as a mixed type CI, and its adsorption onto the MS surface followed Langmuir's isotherm.
- MBZ, at C of 1.061 g/L, exhibited an optimal IE(%) of 96.610% in 0.5 M H_2SO_4, after 48.58 h.
- MBZ is highly efficient for MS surface CI in H_2SO_4.
- DFT and MD studies show that increasing T improved MBZ IE(%), and that its adsorption onto the MS surface was proportional to T, corroborating the findings on T effect and molecular adsorption sections.
- A quartic predictive model Eq. accurately illustrated the reliance of MBZ IE(%) on the investigated independent elements of the inhibition process in the operational environment.

Authors' contributions

F. O. Edoziuno: conceived and designed the analysis; conceptualized ideas; performed the experiment and analysis; analyzed data; wrote the paper- developed some sections of the manuscript. **B. U. Odoni**: performed gravimetric experiments; wrote the paper - developed some sections of the manuscript. **A. A. Adediran**: conceived and designed the analysis: conceptualized ideas; offered key intellectual support, assessed and appraised the manuscript. **S. Byadi**: performed the analysis-MD simulation; analyzed data; wrote the paper - developed some sections of the manuscript. **A. Barhoumi**: performed the analysis - MD simulation; and analyzed data; wrote the paper - developed some sections of the manuscript. **C. C. Nwaeju**: assisted in the predictive modelling, optimization, edition of the manuscript and plagiarism test. **L. U. Modebe**: offered key intellectual support, assessed, reviewed and appraised the manuscript. **J. O. Okeniyi**: performed the analysis; offered key intellectual support, assessed, reviewed and appraised the manuscript.

Abbreviations
AgCl: silver chloride
AIC: Akaike information criterion
ANOVA: analysis of variance
BIC: Bayesian information criterion
$C_7H_6N_2$: benzimidazole
C: concentration
CCD: central composite design
CE: counter electrode
CI: corrosion inhibition/inhibitor
CR: corrosion rate
CV: coefficient of variation
Df: degree of freedom
DFT: density functional theory
DNP: double numerical plus polarization
E_a: activation energy
$E_{binding}$: binding energy
E_{corr}: corrosion potential
$E_{interaction}$: interaction energies
EDXS: energy dispersive X-ray spectroscopy
E_{HOMO}: energy of the highest occupied molecular orbital
E_{LUMO}: energy of the lowest unoccupied molecular orbital
$G°_{ads}$: standard free energy of adsorption
GGA: generalized gradient approximation
H_2SO_4: sulphuric acid
i_{corr}: corrosion current density
IE(%): inhibition efficiency
IT: immersion time
K_{ads}: adsorption equilibrium constant
MBZ: mebendazole (methyl-5-benzoyl-2-benzimidazole: $C_7H_6N_2$ carbamate derivative)
MD: molecular dynamics
MEP: molecular electrostatic potential
MS: mild steel
N110: height of transmitted electrons
PCM: polarized continuum model
PDP: potentiodynamic polarization
Q_{ads}: heat of adsorption
R^2: determination coefficient
redox: reduction and oxidation reactions
RE: reference electrode
RSM: response surface methodology
SCRF: self-consistent reaction field
SD: standard deviation
SEM: scanning electron microscopy
T: temperature
WE: working electrode
WL: weight loss

Kinetic parameters

β_a**:** Tafel anodic slope

β_c**:** Tafel cathodic slope

Δ: energy gap

ΔG°_{ads}: Gibb's free energy of adsorption

ΔN: fraction of transferred electrons

μ: dipolar moment

η_{Fe}: metal hardness

η_{inh}: inhibitor hardness

θ: degree of surface coverage

$\emptyset$**:** work function

χ_{inh}: inhibitor electronegativity

References

1. Loto CA, Popoola API, Fayomi OS et al. Corrosion polarization behaviour of type 316 stainless steel in strong acids and acid chlorides. Int J Electrochem Sci. 2012;7:3787-3797.

2. Bothi Raja P, Sethuraman MG. Inhibitive effect of black pepper extract on the sulphuric acid corrosion of MS. Mater Lett. 2008;(62) 17-18:2977-2979. https://doi.org/10.1016/j.matlet.2008.01.087

3. Nishimura R, Tsuru T, Ohtsuka T et al. Understanding of Corrosion Phenomena : Process, Mechanism, and Method. Int J Corros. 2012:286174. https://doi.org/10.1155/2012/286174

4. Gupta NK, Gopal CSA, Srivastava V et al. Application of expired drugs in corrosion inhibition of MS. Int J Pharm Chem Analyt. 2017;(4)1:8-12. https://doi.org/ 10.18231/2394-2797.2017.0003

5. Peme T, Olasunkanmi LO, Bahadur I et al. Adsorption and corrosion inhibition studies of some selected dyes as corrosion inhibitors for MS in acidic medium: Gravimetric, electrochemical, quantum chemical studies and synergistic effect with iodide ions. Molecules. 2015;20:16004-16029. https://doi.org/10.3390/molecules200916004

6. Ofuyekpone O, Akaluzia RO, Edibo S. Investigating the influence of immersion time and inhibitor C on the inhibiting potential of *Imperata cylindrica* as Corrosion Inhibitor of MS. Int J Res Eng Innov. 2017;1:147-152. http://www.ijrei.com

7. Mashuga ME, Olasunkanmi LO, Adekunle AS et al. Adsorption, thermodynamic and quantum chemical studies of 1-hexyl-3-methylimidazolium based ionic liquids as corrosion inhibitors for MS in HCl. Materials (Basel). 2015;8:3607-3632. https://doi.org/10.3390/ma8063607

8. Finšgar M, Jackson J. Application of corrosion inhibitors for steels in acidic media for the oil and gas industry: A review. Corros Sci. 2014;86:17-41. https://doi.org/10.1016/j.corsci.2014.04.044

9. Nwabanne JT, Okafor VN. Adsorption and thermodynamics study of the inhibition of corrosion of MS in H2SO4 medium using *Vernonia amygdalina*. J Miner Mater Charact Eng. 2012;11:885-890.

10. Sivakumar V, Velumani K, Rameshkumar S. Colocid Dye - A Potential Corrosion Inhibitor for the Corrosion of MS in Acid Media. Mater.Res. 2018:21:4. e20170167. https://doi.org/10.1590/1980-5373-MR-2017-0167

11. Oguzie EE, Li Y, Wang FH. Corrosion inhibition and adsorption behaviour of methionine on MS in sulfuric acid and synergistic effect of iodide ion. J Collo Interf Sci. 2007;310:90-98. https://doi.org/10.1016/j.jcis.2007.01.038

12. Karthikeyan S. Drugs/antibiotics as potential corrosion inhibitors for metals-a review. Int J Chem Tech Res. 2016;(9)6:51-259.

13. Al-Otaibi MS, Al-Mayouf AM, Khan M et al. Corrosion inhibitory action of some plant extracts on the corrosion of MS in acidic media. Arab J Chem. 2014;7:340-346. https://doi.org/10.1016/j.arabjc.2012.01.015

14. Stango SAX, Vijayalakshmi U. Studies on corrosion inhibitory effect and adsorption behaviour of waste materials on MS in acidic medium. J Asian Ceram Soc. 2018;6: 20-29. https://doi.org/10.1080/21870764.2018.1439608

15. Loto RT. Surface coverage and corrosion inhibition effect of Rosmarinus officinalis and zinc oxide on the electrochemical performance of low carbon steel in dilute acid solutions. Results Phys. 2018;8:172-179. https://doi.org/10.1016/j.rinp.2017.12.003

16. Eddy NO, Odoemelam SA, Ekwumemgbo P. Inhibition of the corrosion of MS in H2SO4 by penicillin G. Sci Res Essay. 2009;(4)1:033-038.

17. Loto CA, Loto RT, Osugbunu O et al. Corrosion inhibition effect of *Allium Cepa* extracts on MS in HCL. Der Pharma Chem. 2016;8:20:20-30. http://derpharmachemica.com/archive.html

18. Loto CA, Loto RT, Joseph OO. Effect of benzamide on the corrosion inhibition of MS in sulphuric acid. South Afri J Chem. 2017;70:38-43. https://doi.org/10.17159/0379-4350/2017/v70a6

19. Karthik G, Sundaravadivelu M. Inhibition of MS Corrosion in Sulphuric Acid Using Esomeprazole and the Effect of Iodide Ion Addition. ISRN Electrochem. 2013:1-10. https://doi.org/10.1155/2013/403542

20. Dagdag O, El Harfi A, Cherkaoui O et al. Rheological, electrochemical, surface, DFT and molecular dynamics simulation studies on the anticorrosive properties of new epoxy monomer compound for steel in 1 M HCl solution. RSC Adv. 2019;9:4454. https://doi.org/10.1039/C8RA09446B

21. Oguzie EE, Li Y,. Wang SG et al. Understanding corrosion inhibition mechanisms - Experimental and theoretical approach. RSC Adv. 2011;1: 866-873. https://doi.org/10.1039/c1ra00148e

22. Dagdag O, Safi Z, Erramli H et al. Adsorption and anticorrosive behaviour of aromatic epoxy monomers on carbon steel corrosion in acidic solution: computational studies and sustained experimental studies. RSC Adv. 2019;9:14782-14796. https://doi.org/10.1039/c9ra01672d

23. Paul S, Koley I. Corrosion Inhibition of Carbon Steel in Acidic Environment by Papaya Seed as Green Inhibitor. J. Bio- Tribo-Corros. 2016;2:2-11. https://doi.org/10.1007/s40735-016-0035-2

24. Nahlé A, Abu-Abdoun II, Abdel-Rahman I. Inhibition of MS corrosion by 3-benzoylmethyl benzimidazolium hexafluoroantimonate in acidic solution. Int J Corros. 2012:246013. https://doi.org/10.1155/2012/246013

25. Moreira RR, Soares TF, Ribeiro J. Electrochemical Investigation of Corrosion on AISI 316 Stainless Steel and AISI 1010 Carbon Steel: Study of the Behaviour of Imidazole and Benzimidazole as Corrosion Inhibitors. Adv Chem Eng Sci. 2014;04:503-514. https://doi.org/10.4236/aces.2014.44052

26. Ngobiri NC, Okorosaye-Orubite K. Adsorption and corrosion inhibition characteristics of two medicinal molecules. Chem Int. 2017;(3)2:185-194.

27. Hassan KH, Khadom AA, Kurshed NH. *Citrus aurantium* leaves extracts as a sustainable corrosion inhibitor of MS in sulfuric acid. South Afr J Chem Eng. 2016;22:1-5. https://doi.org/10.1016/j.sajce.2016.07.002

28. Verma C, Chauhan DS, Quraishi MA. Drugs as environmentally benign corrosion inhibitors for ferrous and nonferrous materials in acid environment: An overview. J Mater Environ Sci. 2017;(8)11:4040-4051.

29. Gece G. Drugs: A review of promising novel corrosion inhibitors. Corros. Sci. 2011;53:3873-3898. https://doi.org/10.1016/j.corsci.2011.08.006

30. Ahamad I, Quraishi MA. Mebendazole: New and efficient corrosion inhibitor for MS in acid medium. Corros Sci. 2010;52:651-656. https://doi.org/10.1016/j.corsci.2009.10.012

31. Al-Kurdi Z, Al-Jallad T, Badwan A et al. High-performance liquid chromatography method for determination of methyl-5-benzoyl-2-benzimidazole carbamate (mebendazole) and its main degradation product in pharmaceutical dosage forms. Talanta. 1999;50:1089-1097. https://doi.org/10.1016/S0039-9140(99)00212-X

32. Edoziuno FO, Adediran AA, Odoni BU et al. Performance of Methyl-5-Benzoyl-2-Benzimidazole Carbamate (Mebendazole) as Corrosion Inhibitor for MS in Dilute Sulphuric Acid. Sci World J. 2020:1-11. https://doi.org/10.1155/2020/2756734

33. Odoni BU, Edoziuno FO, Chukwurah NC. Corrosion inhibition potential of methyl-5-benzoyl-2-benzimidazole carbamate (mebendazole) for MS in 1.0m sulphuric acid. Int J Res Eng Innov. 2017;1:190-194. http://www.ijrei.com

34. Edoziuno FO, Odoni BU, Adediran AA et al. Analyses of the Gravimetric and Electrochemical Effects of $C_{16}H_{13}N_3O_3$ on MS Corrosion in 0.5 M H_2SO_4. J Phys Conf Ser. 2019;1378:032064. https://doi.org/10.1088/1742-6596/1378/3/032064

35. Edoziuno FO, Adediran AA, Odoni BU et al. Influence of wormin mebendazole on the corrosion of MS in 1.0M sulphuric acid. Results Eng. 2021;9:100192. https://doi.org/10.1016/j.rineng.2020.100192

36. Edoziuno FO, Adediran AA, Odoni BU Odoni et al. Comparative analysis of corrosion inhibition effects of mebendazole (MBZ) on MS in three different sulphuric acid concentrations. Int J Corros Scale Inhib. 2020;9:1049-1058. https://doi.org/10.17675/2305-6894-2020-9-3-17

37. Xia G, Jiang X, Zhou L et al. Synergic effect of methyl acrylate and N-cetylpyridinium bromide in N-cetyl-3-(2-methoxycarbonylvinyl)pyridinium bromide molecule for X70 steel protection. Corros Sci. 2015;94:224-236. https://doi.org/10.1016/j.corsci.2015.02.005

38. Sadik K, Byadi S, Aboulmouhajir A. Quantum and dynamic investigations of complex iron- alkaloid-extract Cytisine derivatives of *Retama monosperma* (L.) *Boiss*. Seeds as eco-friendly inhibitors for MS corrosion in 1 M HCl. J Mol Struct. 2021(1244)15:130921. https://doi.org/10.1016/j.molstruc.2021.130921

39. Neese F, Wennmohs F, Becker U et al. ORCA 3.0.1 Manual (Input Description), 2014.

40. Cao Z, Tang Y, Cang H et al.Novel benzimidazole derivatives as corrosion inhibitors of MS in the acidic media. Part II: Theoretical studies. Corros Sci. 2014;83: 292-298. https://doi.org/10.1016/j.corsci.2014.02.025

41. Pearson RG. Absolute Electronegativity and Hardness: Application to Inorganic Chemistry. Inorg Chem. 1988;27:734-740. https://doi.org/10.1021/ic00277a030

42. Akkermans RLC, Spenley NA, Robertson SH. Monte carlo methods in materials studio. Mol Simul. 2013;39:1153-1164. https://doi.org/10.1080/08927022.2013.843775

43. Salarvand Z, Amirnasr M, Talebian M et al. Enhanced corrosion resistance of MS in 1 M HCl solution by trace amount of 2-phenyl-benzothiazole derivatives: Experimental, quantum chemical calculations and molecular dynamics (MD) simulation studies. Corros Sci. 2017;114:133-143. https://doi.org/10.1016/j.corsci.2016.11.002

44. Sun H. Compass: An ab initio force-field optimized for condensed-phase applications - Overview with details on alkane and benzene compounds. J Phys Chem B. 1998;102:7338-7364. https://doi.org/10.1021/jp980939v

45. Saha SK, Dutta A, Ghosh P et al. Novel Schiff-base molecules as efficient corrosion inhibitors for MS surface in 1 M HCl medium: Experimental and theoretical approach. Phys Chem Phys. 2016;(18)27:17898-17911. https://doi.org/10.1039/c6cp01993e

46. Saha SK, Dutta A, Ghosh P et al. Adsorption and corrosion inhibition effect of schiff base molecules on the MS surface in 1 M HCL medium: A combined experimental and theoretical approach. Phys Chem. 2015;17:5679-5690. https://doi.org/10.1039/c4cp05614k

47. Anadebe VC, Onukwuli OD, Omotioma M et al. Optimization and Electrochemical Study on the Control of MS Corrosion in Hydrochloric Acid Solution with *Bitter Kola* Leaf Extract as Inhibitor. South Afr J Chem. 2018;71:51-61. https://doi.org/10.17159/0379-4350/2018/v71a7

48. Omotioma M, Onukwuli OD. Modeling the Corrosion Inhibition of MS in HCl Medium with the Inhibitor of Pawpaw Leaves Extract. Port Electrochim Acta. 2016;34: 287-294. https://doi.org/10.4152/pea.201604287

49. Gutiérrez E, Rodríguez JA, Cruz-borbolla J et al. Development of a predictive model for corrosion inhibition of carbon steel by imidazole and benzimidazole derivatives. Corros Sci. 2016;108:23-35. https://doi.org/10.1016/j.corsci.2016.02.036

50. Edoziuno FO, Adediran AA, Odoni BU et al. Optimization and development of predictive models for the corrosion inhibition of MS in sulphuric acid by methyl-5-benzoyl-2-benzimidazole carbamate (mebendazole). Cogent Eng. 2020;7:1714100. https://doi.org/10.1080/23311916.2020.1714100

51. Raducka A, Czylkowska A, Gobis K et al. Characterization of Metal-Bound Benzimidazole Derivatives, Effects on Tumor Cells of Lung Cancer. Materials (Basel). 2021;14:2958. https://doi.org/10.3390/ma14112958

52. Oturak H, Kınaytürk NK, Çırak Ç . Experimental and Theoretical Spectral (FT-IR, Raman, NMR, UV-Vis and NLO) Analysis of a potential antitumor drug: 1-Methyl-6-Nitro-1H-Benzimidazole. Spectrosc Spectr Analyt. 2018;(38)6:1963. https://doi.org/10.3964/j.issn.1000-0593(2018)06-1963-07

53. Popova A, Sokolova E, Raicheva S et al. AC and DC study of the temperature effect on MS corrosion in acid media in the presence of benzimidazole derivatives. Corros Sci. 2003;45:33-58. https://doi.org/10.1016/S0010-938X(02)00072-0

54. Sherif ESM. Corrosion inhibition in 2.0 M sulfuric acid solutions of high strength maraging steel by aminophenyl tetrazole as a corrosion inhibitor. Appl Surf Sci. 2014;292:190-196. https://doi.org/10.1016/j.apsusc.2013.11.110

55. Sherif ESM, Abbas AT, Halfa H et al. Corrosion of high strength steel in concentrated sulfuric acid pickling solutions and its inhibition by 3-amino-5-mercapto-1,2,3-triazole. Int J Electrochem Sci. 2015;10:1777-1791. https://doi.org/10.13140/RG.2.2.10951.91046

56. Sherif ESM, Abbas AT, Gopi D et al. Corrosion and Corrosion Inhibition of High Strength Low Alloy Steel in 2.0 M Sulfuric Acid Solutions by 3-Amino-1,2,3-triazole as a Corrosion Inhibitor. J Chem. 2014. https://doi.org/10.1155/2014/538794

57. Loto CA, Joseph OO, Loto RT. Inhibition effect of *Vernonia amygdalina* extract on the corrosion of MS reinforcement in concrete in 0.2 M H_2SO_4 Environment. Eur J Environ Civ Eng. 2013;17:10:1026-1038. https://doi.org/10.1080/19648189.2013.841596

58. Loto CA, Joseph OO, Loto RT. Inhibition effect of zinc oxide on the electrochemical corrosion of MS reinforced concrete in 0.2 M H_2SO_4. J. Mater Environ Sci. 2016;7:915-925.

59. Riggs jr. OL. Corrosion Inhibition, Second ed, C.C. Nathan, Houston, TX, 1973.

60. Nnanna LA, Owate IO, Oguzie EE. Inhibition of MS Corrosion in HCl Solution by Pentaclethra macrophylla Bentham Extract. Int J Mater Eng. 2014;4:171-179. https://doi.org/10.5923/j.ijme.20140405.02

61. Olawale O, Adediran AA, Talabi SI et al. Inhibitory action of *Vernonia amygdalina* extract (VAE) on the corrosion of carbon steel in acidic medium. J Electrochem Sci Eng. 2017;7:145-152. https://doi.org/10.5599/jese.353

62. Popova A. Temperature effect on MS corrosion in acid media in presence of azoles. Corros Sci. 2007;49:2144-2158. https://doi.org/10.1016/j.corsci.2006.10.020

63. Chidiebere MA, Nnanna L, Blessing AC et al. Inhibition of Acid Corrosion of MS Using *Delonix Regia* Leaves Extract. 2016;69:74-86. https://doi.org/10.18052/www.scipress.com/ILCPA.69.74

64. Louadi YE, Abrigach F, Bouyanzer A et al. Theoretical and experimental studies on the corrosion inhibition corrosion current density of two tetrakis pyrazole derivatives for MS in 1.0 M HCl. Port Electrochim Acta. 2017;35:159-178. https://doi.org/10.4152/pea.201703159

65. Olasunkanmi LO, Obot IB, Kabanda MM et al. Some quinoxalin-6-yl derivatives as corrosion inhibitors for MS in hydrochloric acid: Experimental and theoretical studies. J Phys Chem C. 2015;119:16004-16019. https://doi.org/10.1021/acs.jpcc.5b03285

66. Pais M, Shwetha N, Rao P. Experimental and Theoretical Evaluation of Efficacy of Inhibitory Action of Benzyl Isothiocyanate Prot. Met. Phys Chem Surfaces. 2021;57:597-607. https://doi.org/10.1134/S2070205121030187

67. Benhiba F, Hsissou R, Benzekri Z et al. DFT/electronic scale. MD simulation and evaluation of 6-methyl-2-(p-tolyl)-1,4-dihydroquinoxaline as a potential corrosion inhibition. J Mol Liq. 2021;335:116539. https://doi.org/10.1016/j.molliq.2021.116539

68. Rodríguez JA, Cruz-Borbolla J, Arizpe-Carreón PA et al. Mathematical models generated for the prediction of corrosion inhibition using different theoretical chemistry simulations. Materials (Basel). 2020;13:5656. https://doi.org/10.3390/ma13245656

69. Laabaissi T, Benhiba F, Rouifi Z et al. Benzodiazepine Derivatives as Corrosion Inhibitors of Carbon Steel in HCl Media: Electrochemical and Theoretical Studies Prot. Met Phys Chem Surfaces. 2019;55:986-1000. https://doi.org/10.1134/S2070205119050149

70. Oguike RS, Kolo AM, Shibdawa AM et al. Density Functional Theory of MS Corrosion in Acidic Media Using Dyes as Inhibitor: Adsorption onto Fe(110) from Gas Phase. ISRN Phys Chem. 2013. https://doi.org/10.1155/2013/175910

71. Contreras RR, Fuentealba P, Galvan M et al. A direct evaluation of regional Fukui functions in molecules. Chem Phys Lett. 1999;(304)5-6:405-413. https://doi.org/10.1016/S0009-2614(99)00325-5

72. Rahmani H, Alaoui KI, El Azzouzi M, et al. Corrosion assessment of MS in acid environment using novel triazole derivative as an anti-corrosion agent: A combined experimental and quantum chemical study. Chem Data Collect. 2019;24: 100302. https://doi.org/10.1016/j.cdc.2019.100302.

73. Singh A, Ansari KR, Haque J et al. Effect of electron-donating functional groups on corrosion inhibition of MS in hydrochloric acid: Experimental and quantum chemical study. J Taiwan Inst Chem Eng. 2018;82: 233-251.

74. Kothari CR, Garg G. Research Methodology: Methods and Techniques, 3rd ed., New Age International (P) Ltd., Publishers, New Delhi, 2014.